

# SUPERNOVAE FROM DIRECT COLLISIONS OF WHITE DWARFS AND THE ROLE OF HELIUM SHELL IGNITION

ODED PAPISH & HAGAI BINYAMIN PERETS

Technion - Israel Institute of Technology, physics department, Haifa, Israel 32000

*Draft version June 7, 2021*

## Abstract

Models for supernovae (SNe) arising from thermonuclear explosions of white dwarfs (WDs) have been extensively studied over the last few decades, mostly focusing on the single degenerate (accretion of material of a WD) and double degenerate (WD-WD merger) scenarios. In recent years it was suggested that WD-WD direct collisions provide an additional channel for such explosions. Here we extend the studies of such explosions, and explore the role of Helium-shells in affecting the thermonuclear explosions. We study both the impact of low-mass helium ( $\sim 0.01 M_{\odot}$ ) shells, as well as high mass shells ( $\geq 0.1 M_{\odot}$ ). We find that detonation of the massive helium layers precede the detonation of the WD Carbon-Oxygen (CO) bulk during the collision and can change the explosive evolution and outcomes for the cases of high mass He-shells. In particular, the He-shell detonation propagates on the WD surface and inefficiently burns material prior to the CO detonation that later follows in the central parts of the WD. Such evolution leads to larger production of intermediate elements, producing larger yields of  $^{44}\text{Ti}$  and  $^{48}\text{Cr}$  relative to the pure CO-CO WD collisions. Collisions of WDs with a low-mass He-shell do not give rise to helium detonation, but helium burning does precede the CO bulk detonation. Such collisions produce a high velocity, low-mass of ejected burned material enriched with intermediate elements, with smaller changes to the overall explosion outcomes. The various effects arising from the contribution of low/high mass He layers change the kinematics and the morphological structure of collision-induced SNe and may thereby provide unique observational signatures for such SNe, and play a role in the chemical enrichment of galaxies and the production of intermediate elements and positrons from their longer-term decay.

## 1. INTRODUCTION

Thermonuclear explosions of white dwarfs (WDs) have been extensively studied over the last decades, and are thought to be the progenitors of various types of supernovae (SNe), most notably type Ia SNe, but possibly also calcium-rich faint type Ib SNe (Perets et al. 2010). Models for thermonuclear detonations are traditionally divided between double degenerate (DD) models and single degenerate models (SD). The former focus on cases of mergers of two WDs, and the latter on accretion of material from a companion star onto a WD (See Maoz et al. 2014 for a review). In recent years it was suggested that the DD scenario can be extended to WD-WD *collisions* and not only mergers, but the former were thought to be extremely rare, and occur only in dense stellar clusters. For this reason they attracted relatively little attention compared with other WD explosion progenitors. Such collisions, however, are likely to be observable as type Ia SNe (Rosswog et al. 2009) and possibly non-standard SNe (Raskin et al. 2009, 2010). Recently, it was shown that some triple systems may dynamically evolve through a quasi-secular process, reminiscent of Kozai-Lidov oscillations (Kozai 1962; Lidov 1962), but where significant peri-center changes can occur on a single orbit time-scale Antonini & Perets (2012), leading to extremely close peri-center approaches. In particular, it was suggested that such evolution in triples hosting an inner WD-WD binary could lead to physical collisions and the production of type Ia SNe (Thompson 2011; Katz & Dong 2012; Kushnir et al. 2013). Though such systems are not likely to be frequent (e.g. Hamers et al. (2013); see also section 4.3 in the following), they may

be much more frequent than WD-WD collisions in dense clusters, making such scenarios more likely.

While previous studies mostly focused on collisions of carbon-oxygen (CO), the potential role of a He component, and in particular He-shells on CO-WDs attracted only little attention. Kushnir & Katz (2014) calculated the conditions for a detonation in a tiny helium shell around two  $1M_{\odot}$  WDs and concluded that detonation cannot occur during the collision. Realistic CO WDs typically hold outer Helium layers which can range in mass between  $10^{-3} M_{\odot}$  for more massive WDs up to  $0.024 M_{\odot}$  for the lowest mass CO WDs (Lawlor & MacDonald 2006). In the case of an interacting binary where a WD grows through accretion, the accreting WD might have a significant outer Helium layer of up to  $0.1 M_{\odot}$  or more on low mass WD (e.g. Bildsten et al. 2007); such a helium layer is thought to play a major role in the SD sub-Chandrasekhar and .Ia models for thermonuclear explosions (Woosley et al. 1986; Livne & Glasner 1991; Bildsten et al. 2007; Shen & Bildsten 2009; Perets et al. 2010; Waldman et al. 2011); the helium layer may ignite and later possibly induce the detonation of the CO-WD bulk through converging shock (Shen & Bildsten 2014). Recently, it was suggested to play a similar role in WD-WD mergers Pakmor et al. (2013). Here we study the outcomes of WD-WD collisions and explore the possibility that a helium shell can play an important role in such collisions. As we discuss in the following, a He-shell can produce non-negligible effects on the collisions outcome, changing the composition, energetics and velocity distributions of the resulting SN; the amplitude of these effects depend on the mass of the He layer considered, with more

significant effects arising from larger He layers.

We begin by describing our 2D simulations and their initial conditions (section 2), and present the main results in section 3. We then discuss our results (section 4), where we also discuss the rates of such collisions and point out their main implications and their observational signatures.

## 2. SIMULATIONS

### 2.1. WD Models

The WD models are calculated using the MESA stellar evolution code (Paxton et al. 2011). The initial WD models were taken from Wolf et al. (2013) and then changed using MESA for the different compositions. The models with a small helium shell were built by relaxing the chemical composition of the non helium elements to be 50% carbon and 50% oxygen. For the CO models we removed the helium shell up to a total of  $10^{-3}M_{\odot}$ . After that we relaxed the WDs composition to be 50% carbon and 50% oxygen. The models with a large helium shell were built by accretion at a rate of  $10^{-8}M_{\odot}\text{yr}^{-1}$  of helium to the initial models up to a total  $0.1M_{\odot} - 0.2M_{\odot}$  of helium on the WDs. In the following we consider the whole range of low-mass to high mass helium shells, but we should note that the latter cases of massive shells are likely to be rare. Nevertheless, even massive helium shells may exist around WDs in binaries with a helium donor star (e.g. AM-CVn systems), and the possibility of helium shell detonation in such cases has been widely explored (e.g. Woosley et al. 1986; Livne & Glasner 1991; Waldman et al. 2011, and references therein). A collision of a CO WD with such a WD with a massive helium shell could therefore occur either randomly in dense clusters, or in high multiplicity systems ( $>2$  component) in which one of the components is such a helium accreting WD in a close binary, and another outer CO WD companion exists (e.g. Krzemiński 1972 find a triple system with an inner AM CVn). The outer WD do not need to be close, as even collisions with very far companions could occur in the field (Michaely & Perets 2015).

### 2.2. Hydrodynamical Simulations

We carried 17 different 2D simulations of WD-WD head-on collisions using the FLASH v4.2 code (Fryxell et al. 2000). The widely used FLASH code is a publicly available code for supersonic flow suitable for astrophysical applications. The simulations were done using the unsplit PPM solver of FLASH in 2D axisymmetric cylindrical coordinates on a grid of size  $3.2 \times 6.4$  [ $10^{10}\text{cm}$ ] using adaptive mesh refinement (AMR). To prevent the production of unreal early detonation that may arise from numerical resolution we applied a limiter approach following Kushnir et al. (2013). We made multiple simulations with increased resolution until convergence was reached in the nuclear burning. We found a resolution of  $5 - 10\text{km}$  to be sufficient for convergence to up to 10%. Gravity was included as a multipole expansion of up to multipole  $l = 10$  using the new FLASH multipole solver. The equation of state used in the simulations is the Helmholtz EOS (Timmes & Swesty 2000). This EOS includes contributions from partial degenerate electrons and positrons, radiation, and non degenerate ions. The nuclear network was FLASH's 19

Model	Primary Mass [ $M_{\odot}$ ]	$\rho_c$ [g]	Secondary Mass [ $M_{\odot}$ ]	$\rho_c$ [g]
1A	0.6 CO	$3.4 \times 10^6$	0.6 CO	$3.4 \times 10^6$
1B	0.6 CO	$3.4 \times 10^6$	0.6 CO + 0.01 He	$3.5 \times 10^6$
1C	0.6 CO + 0.01 He	$3.5 \times 10^6$	0.6 CO + 0.01 He	$3.5 \times 10^6$
1D	0.6 CO + 0.024 He	$4.0 \times 10^6$	0.6 CO + 0.024 He	$4.0 \times 10^6$
1E	0.6 CO	$3.4 \times 10^6$	0.6 CO + 0.1 He	$5.7 \times 10^6$
1F	0.6 CO + 0.1 He	$5.7 \times 10^6$	0.6 CO + 0.1 He	$5.7 \times 10^6$
1G	0.6 CO + 0.2 He	$1.1 \times 10^7$	0.6 CO + 0.2 He	$1.1 \times 10^7$
2A	0.7 CO	$5.9 \times 10^6$	0.7 CO	$5.9 \times 10^6$
2B	0.7 CO	$5.9 \times 10^6$	0.7 CO + 0.01 He	$6.1 \times 10^6$
2C	0.7 CO + 0.01 He	$6.1 \times 10^6$	0.7 CO + 0.01 He	$6.1 \times 10^6$
2D	0.7 CO + 0.024 He	$6.8 \times 10^6$	0.7 CO + 0.024 He	$6.8 \times 10^6$
2E	0.7 CO	$5.9 \times 10^6$	0.7 CO + 0.1 He	$9.9 \times 10^6$
3	0.6 CO	$3.4 \times 10^6$	0.7 CO	$5.9 \times 10^6$
4	0.7 CO	$5.9 \times 10^6$	0.8 CO	$1.0 \times 10^7$
5A	0.8 CO	$1.0 \times 10^7$	0.6 CO	$3.4 \times 10^6$
5B	0.8 CO	$1.0 \times 10^7$	0.6 CO + 0.01 He	$3.5 \times 10^6$
5C	0.8 CO	$1.0 \times 10^7$	0.6 CO + 0.1 He	$5.7 \times 10^6$

TABLE 1  
COLLISION MODELS.

isotopes alpha chain network. This network can capture well the energy generated during the nuclear burning (Timmes et al. 2000). As initial conditions we take the two WDs to be at contact with free fall velocities. The various simulations conducted are summarized in table 1.

## 3. RESULTS

### 3.1. Collisions of pure CO-WDs and comparison with previous collision simulations

We run several pure CO-WDs collisions in order to check the consistency of our simulations with previous works, and then use them as a benchmark for comparison with the novel collision simulations in which WDs with He-layers were considered.

Previous collision simulations include several works by different groups (Rosswog et al. 2009; Raskin et al. 2009, 2010; Lorén-Aguilar et al. 2010; Hawley et al. 2012; Kushnir et al. 2013; García-Senz et al. 2013). In these simulations only pure CO-WD collisions were simulated (or CO-WD - He-WD collisions Rosswog et al. 2009). Early studies of WD-WD collisions showed large discrepancies in the  $^{56}\text{Ni}$  yields produced, likely resulting from insufficient resolution (Kushnir et al. 2013) and the use of too-large time steps in coupling the nuclear burning to the hydrodynamics (Hawley et al. 2012). Kushnir et al. (2013) devised the limiter approach to tackle such potential difficulties; recent high resolutions (e.g., García-Senz et al. 2013) show a convergence to Kushnir et al. (2013) results, supporting the validity of their limiter approach. Our main comparison is therefore with the results by Kushnir et al. (2013), who similarly used the FLASH code, and included the limiter approach. One difference in our simulations is the use of the unsplit hydro solver in FLASH while Kushnir et al. 2013 uses the split solver.

Our pure CO-WDs collisions result in CO detonations in both WDs. The total energy  $E_k$  and abundances of helium, intermediate elements, and nickel are presented in Table 3.2. All the results are shown after the nuclear reactions in the simulations ended.  $E_k$  includes ki-

netic, thermal, and gravitational energy. The amount of nickel and total energy we get is similar to the results of Kushnir et al. (2013). This is expected as in both works the same code is used with the same limiter on the nuclear reaction rate. We find our results to be similar up to  $\sim 10\%$  in the pure CO cases. These small differences should exist as a result of the slightly different initial preparation of the progenitors and the resolutions used in the two studies. We therefore confirm previous studies of such collisions and find them to be consistent with the results we obtain

### 3.2. Collisions between CO-WDs with a low-mass, non-detonating helium layer

Collisions of WDs with low-mass helium layers (up to  $M_{\text{He}} < 0.024M_{\odot}$ ; see Fig. 1) do not give rise to a detonation in the helium layer. Such collisions are characterized by three phases: a) The helium compression phase. A short time after the collision the helium layer is compressed to densities of  $\rho_{\text{He}} \approx 10^5 \text{ g cm}^{-3}$  and temperatures of  $T_{\text{He}} \approx 10^9 \text{ K}$ . Under these conditions the helium stars burning, but no detonation is triggered. The compressed helium is ejected in the plane perpendicular to the collision direction with velocities of up to  $20,000 \text{ km s}^{-1}$  as it burns to intermediate elements. b) The CO detonation phase. This phase is very similar to the pure CO-WDs collisions. The compression and burning of the helium layer has almost no effect on the CO core. The detonation in the CO material is triggered in a very similar way to pure CO-CO collisions (Kushnir et al. 2013) and can be seen in Fig. 1. c) Outer helium layer ejection. The detonation wave in the CO material reaches the outer part of the helium layer and eject the partially burned helium layer. At the end of the explosion  $\sim 1/2$  of the initial helium mass survives in all cases and is ejected after the shock reaches the outer part of the WD. Intermediate mass elements are also ejected in this way. The  $^{56}\text{Ni}$  yields in all cases are comparable to the  $^{56}\text{Ni}$  yield in pure CO-CO collisions. The total mass of the intermediate elements is summarized in table 3.2. We caution that exact outcomes of these simulations depend on the nucleosynthetic network used. Here we use the 19 isotopes alpha chain network; in section 3.4 we show that although the simplified smaller network well captures the overall evolution, energetics and nucleosynthetic production, the result obtained differ quantitatively (and non-negligibly) from those obtained using a much larger network. In particular, the latter show an increase of the nickel production and suppression of the IME production, compared with the results of the smaller network.

### 3.3. Induced helium detonation in collisions between CO-WD with a large-mass helium layer

In collisions of WDs with a massive ( $M_{\text{He}} \geq 0.024M_{\odot}$ ) helium layers, the helium detonates during its compression phase. For the  $M_{\text{He}} = 0.024M_{\odot}$  case the helium detonation is not able to propagate through the curved helium shell (Fig. 2) and has almost no influence on the overall collision outcomes, i.e. the detonation in the CO core is triggered by the collision in a similar way to pure CO-WDs collisions. For more massive shells ( $M_{\text{He}} = 0.1M_{\odot}$ ; models 1F,2E) the helium detonation is

Model	$^4\text{He}$	$^{40}\text{Ca}$	$^{44}\text{Ti}$	$^{48}\text{Cr}$	$^{56}\text{Ni}$	$E_{\text{exp}}$	Helium Detonation
1A	1(-3)	4(-2)	9(-5)	4(-4)	0.31	1.3	-
1B	5(-3)	4(-2)	1.5(-3)	1(-3)	0.27	1.3	No
1C	1(-2)	5(-2)	3(-3)	2(-3)	0.29	1.3	No
1D	3(-2)	4(-2)	5(-3)	3(-3)	0.38	1.2	Yes
1E	4(-2)	4(-2)	1.3(-2)	1(-2)	0.4	1.4	Yes
1F	1(-1)	4(-2)	2(-2)	2(-2)	0.8	1.8	Yes
1G	1(-1)	6(-2)	7(-3)	9(-3)	0.3	2.1	Yes
2A	3(-3)	5(-2)	1(-4)	6(-4)	0.52	1.5	-
2B	6(-3)	4(-2)	8(-4)	9(-4)	0.65	1.7	No
2C	8(-3)	5(-2)	1.5(-3)	1(-3)	0.54	1.6	No
2D	3(-2)	5(-2)	3(-3)	3(-3)	0.61	1.6	Yes
2E	5(-2)	5(-2)	1.4(-2)	1(-2)	0.67	1.6	Yes
3	2(-3)	4(-2)	1(-4)	5(-4)	0.42	1.4	-
4	1(-3)	4(-2)	1.6(-4)	6(-4)	0.49	1.6	-
5A	2(-3)	3(-2)	4(-5)	3(-4)	0.32	1.4	-
5B	7(-3)	4(-2)	1(-3)	6(-4)	0.27	1.4	No
5C	5(-2)	6(-2)	1.5(-2)	1(-2)	0.4	1.7	Yes

TABLE 2  
ABUNDANCES AT THE END OF THE SIMULATIONS IN VALUES OF  $M_{\odot}$ . ENERGY IS IN  $10^{51}$  erg.

able to propagate through the shell before the CO is detonated (see Fig. 4). In this case we find that the helium shell burning results in the production of non-negligible amounts of intermediate mass elements and nickel. The velocity of the helium-burned material is lower than the velocity of the material ejected following the CO core detonation which gradually outruns the material ejected through the earlier He-detonation in the shell. For even more massive helium shells ( $M_{\text{He}} = 0.2M_{\odot}$ ; model 1G) the converging shock caused by the helium detonation is able to detonate the CO. In this case the induced CO detonation is obtained earlier than the corresponding CO detonation in the pure CO-CO WD collisions and both

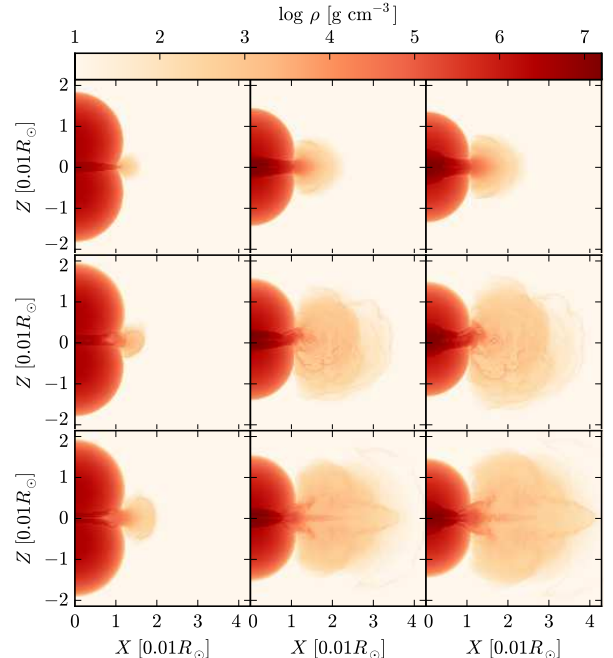


FIG. 1.— Density before, during, and after CO detonation for two  $0.6M_{\odot}$  WDs. Upper panels: pure CO WDs. Middle panels: the top WD with  $0.01M_{\odot}$  of helium while the bottom WD is a pure CO. Bottom panels: both WDs with a layer of  $0.01M_{\odot}$  of helium. The detonation in the CO is similar in the three cases.

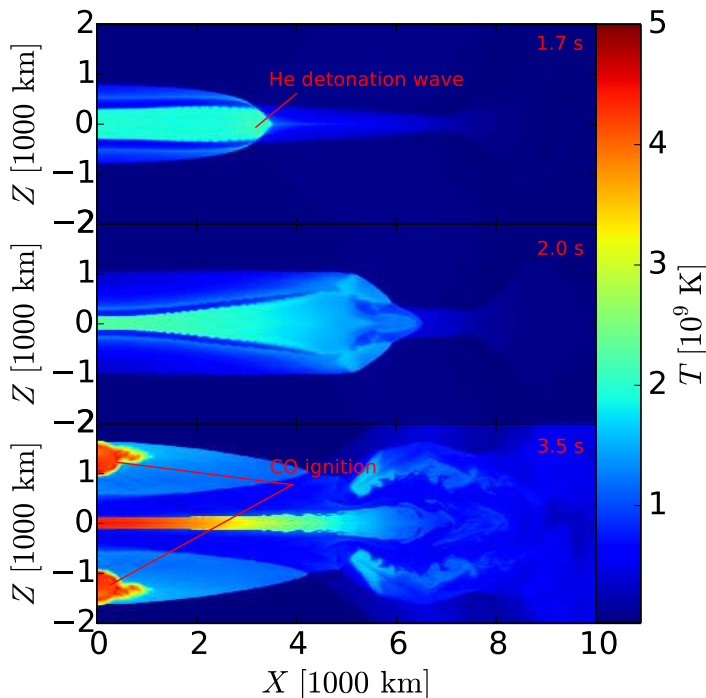


FIG. 2.— Ignition in the He layer and C/O core of two WDs with composition of  $0.6M_{\odot}$  C/O and  $0.024M_{\odot}$  of He. The helium layer is detonated first resulting in a fast ejecta in the horizontal plan. The helium detonation front is not able to propagate along the curved helium shell. The helium ignition has no real effect on the CO ignition process.

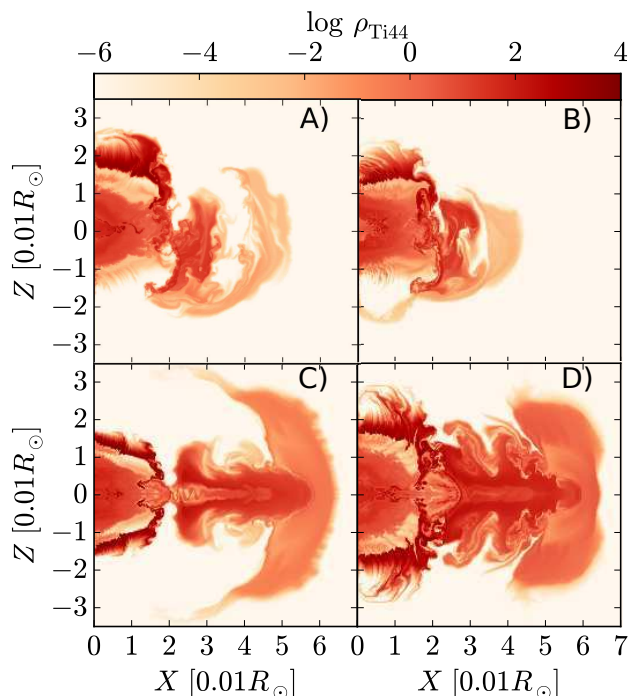


FIG. 3.— Density of  $^{44}\text{Ti}$  after the shock reaches the outer parts of the WDs. A) Top WD is a  $0.6M_{\odot}$  CO with  $0.01M_{\odot}$  of helium; bottom WD is a pure  $0.6M_{\odot}$  CO WD. B) Top WD is a  $0.7M_{\odot}$  CO with  $0.01M_{\odot}$  of helium; bottom WD is a pure  $0.7M_{\odot}$  CO WD. C) Both WDs are  $0.6M_{\odot}$  CO with  $0.01M_{\odot}$  of helium. D) Both WDs are  $0.6M_{\odot}$  CO with  $0.024M_{\odot}$  of helium. Most of the ejected  $^{44}\text{Ti}$  is from the outer parts of the WDs from partial burning of the helium layer. A small plump is ejected during the collision and can be seen in front of the WDs.

the nickel abundance ( $M_{\text{Ni}^{56}} \simeq 0.3M_{\odot}$ ) and the abundance of intermediate elements are smaller than in the pure CO collisions.

### 3.4. Nuclear reactions post-processing

In order to provide a better understanding of the nucleosynthetic yields from WD-WD collisions we go beyond previous models using a small nuclear reaction networks networks. We extend these by including a large 160 post-processed nuclear reaction network for two of our simulations, a pure CO-CO collision (1A) and a CO+He-CO+He (low-mass helium shell) collision (1C). The post-processing was done by including 30,000 trace particles to the simulations and record their thermodynamical conditions throughout the simulations. We post-processed the results from the trace particles using the burn unit of the MESA code (version 7624) (Paxton et al. 2015). MESA uses the JINA reaclib version V2.0 2013-04-02 (Cyburt et al. 2010) database for nuclear reaction rates. The results are summarized in table 3.

The results show production of a larger amount of  $^{56}\text{Ni}$  and suppression of  $^{44}\text{Ti}$  with respect to the results obtained using the smaller  $\alpha$  network in FLASH (19). Similar differences due to the use of larger nucleosynthetic network have been seen in other works (García-Senz et al. 2013), which arise due to the more efficient nuclear burning, producing larger abundances of higher elements (e.g.,  $^{56}\text{Ni}$ ) and lower amounts of intermediate elements (e.g.,  $^{44}\text{Ti}$ ).

### 3.5. Influence of initial separation of the WDs

The simulations in this study were initiated when the two WDs are at contact, and the effect of tidal distortion of the WDs prior to contact were not taken into account. To verify whether such pre-impact effect play a role in the collision outcomes we ran an additional simulation, identical to 1C, but with an initial separation of  $3(R_{\text{WD1}} + R_{\text{WD2}})$ . The results show vary little compares with those obtained from ‘initial contact’ simulations, in particular there only a very small distortion is observed in the WDs structure prior to impact. This is anticipated as the free fall velocity is supersonic and the WDs do not have sufficient time to be significantly distorted by much before the collision. In summary, the energetics, overall evolution post impact and nucleosynthetic yields show only very slight deviations from the ‘initial contact’ simulations.

## 4. DISCUSSION

### 4.1. Composition, morphology and kinematics

In our simulations of WD-WD collisions including a He-layer we find that the helium is burned mostly into intermediate elements resulting in a much higher mass ejecta of these elements compared with pure CO collisions. Only a small fraction of the helium shell burns into  $^{56}\text{Ni}$ , which has only a minor effect on the  $^{56}\text{Ni}$  yields. The deviation in the yield of intermediate elements compared with their yield in pure CO collisions is found to be almost linearly dependent on the He mass (Fig. 5). Using LS fit we find the relation  $M_{\text{He4}} = 0.001883 + 0.462991M_{\text{shell}}$ , i.e., almost half of the helium is left unburned. For  $^{44}\text{Ti}$  and  $^{48}\text{Cr}$  we find  $M_{\text{Ti44}} = (0.132099 \pm 0.006176)M_{\text{shell}}$ ,  $M_{\text{Cr48}} = (0.094573 \pm 0.003914)M_{\text{shell}}$ .



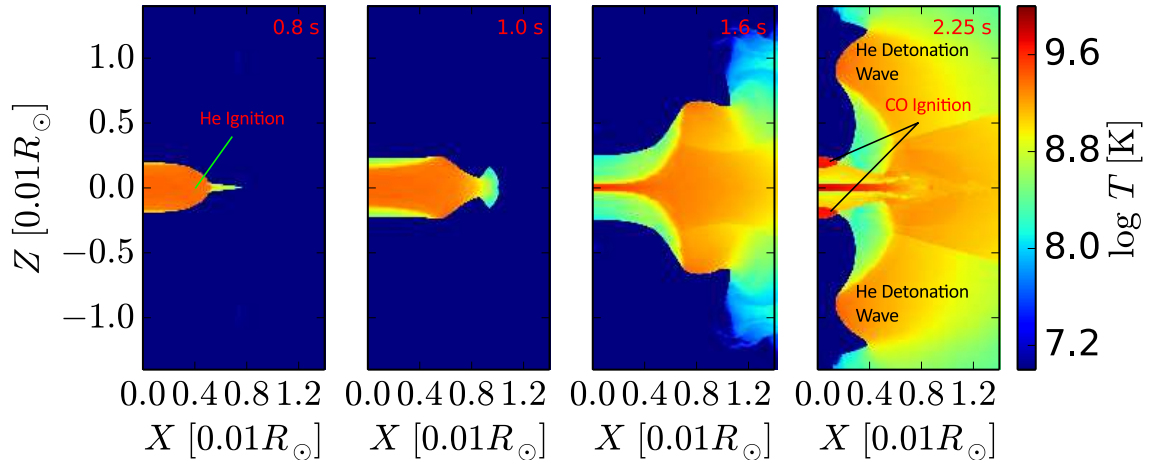


FIG. 4.— Ignition in the Helium shell and the CO core of two WDs with composition of  $0.6M_{\odot}$  CO and  $0.1M_{\odot}$  of He. The helium layer detonates first and propagate along the outer shell. The CO core is then ignited as a result of the collision's shock.

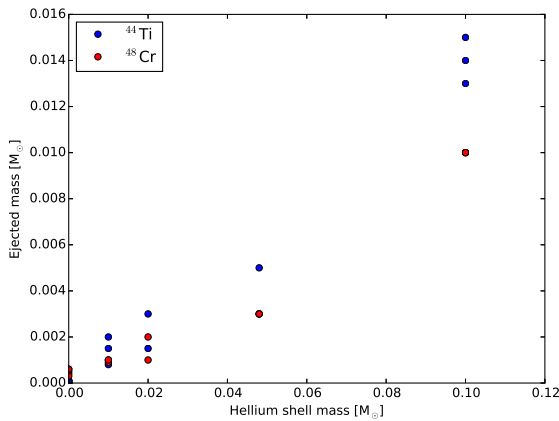


FIG. 5.— Mass ejecta of  $^{44}\text{Ti}$  and  $^{48}\text{Cr}$  for the different models. The lower left points are for pure CO-WD collisions.

For helium shells with mass  $M_{\text{shell}} < 10^{-3}M_{\odot}$  these yields are significantly higher than those produced in collisions of bare CO white dwarfs. For low mass shells the helium ejecta mostly burns as a result of the CO detonation shock and the ejecta is relatively spherically symmetric besides a small ejected plume of He/He-burned material (see Fig. 3). However, a bipolar structure is formed when the two helium shells on the corresponding two WDs have different masses (Fig 3). In the high mass cases most of the burning results from the helium detonation wave. A large fraction of intermediate elements are then ejected in a cone of  $\approx 30^\circ$  to the collision plane.

The velocity distribution of the various components also differs between the different type of collisions. In Fig. 6 we present the velocity profiles for cases 1A, 1B, 1F in the upper, middle, and lower parts of the simulation domain. Collisions which include He-layers show high velocity tails of ejecta of intermediate elements. In particular the most He-rich collisions give rise to a non-negligible mass of material ejected at higher velocities due to the He-detonation stage. Using a much larger nuclear network (see section 3.4) we find a reduction of IME production and an increase of nickel production, showing that a large nuclear network is required for producing the correct abundances (see also Holcomb & Kushnir 2015 for pointing out these issues in a similar context).

#### 4.2. Comparison with other models of type Ia

The overall energetics and behavior of the WD-collision models can be relatively similar to other models for type Ia SNe. However, high yields of intermediate elements do not show in models of the single degenerate scenario. For example, model W7 of Nomoto et al. (1984) results with  $< 10^{-4}M_{\odot}$  of  $^{44}\text{Ti}$  and  $< 10^{-5}M_{\odot}$  of  $^{48}\text{Cr}$ . As the amount of helium on a Chandrasekhar mass WD is small we do not expect high yields of these elements in any case except maybe for a failed Ia supernova (e.g., Jordan et al. 2012; Kromer et al. 2013; this result might also be apply to the core-degenerate scenario Livio & Riess 2003; Kashi & Soker 2011).

In the double degenerate scenario a helium shell can exist on the WDs. Raskin et al. (2012) simulated the merger of two WDs with a helium layer; they found that a detonation occurs in the helium layer when the primary mass was  $1.06M_{\odot}$ ; however it did not lead to carbon detonation as a result of the helium detonation. Pakmor et al. (2013) found that a violent merger with a  $0.01M_{\odot}$  helium shell produces less than  $2 \times 10^{-8}M_{\odot}$  of elements more massive than calcium in the helium shell.

The relatively large abundances of intermediate elements such as  $^{44}\text{Ti}$  can provide a more unique signature for He-rich collisions, though high abundances of these components can also be produced in the SD sub-Chandrasekhar and .Ia explosion models (Woosley et al. 1986; Livne & Glasner 1991; Bildsten et al. 2007; Shen & Bildsten 2009; Perets et al. 2010; Waldman et al. 2011)). Interestingly, recent observations (Troja et al. 2014) suggest that the  $^{44}\text{Ti}$  abundances in Tycho SN remnant are comparable with the abundances we find in the Helium rich collisions (even those with low-mass He-layer). Lopez et al. (2015) did not detect any  $^{44}\text{Ti}$  but only derived upper limits of  $2.4 \times 10^{-4} M_{\odot}$ . Such  $^{44}\text{Ti}$  levels are significantly higher than expected in typical SD scenarios (and much larger than the W7 model), but are still consistent with the main models (1B,2B); and are lower than the sub-Chandrasekhar models (depending on the assumed distance of the Tycho SNR; see figure 4 in Troja et al. 2014). If  $^{44}\text{Ti}$  rich SNe are frequent, then their large production of  $^{44}\text{Ti}$  could also be important for the 511 keV emission in the Galaxy due to positron-electron annihilation fol-

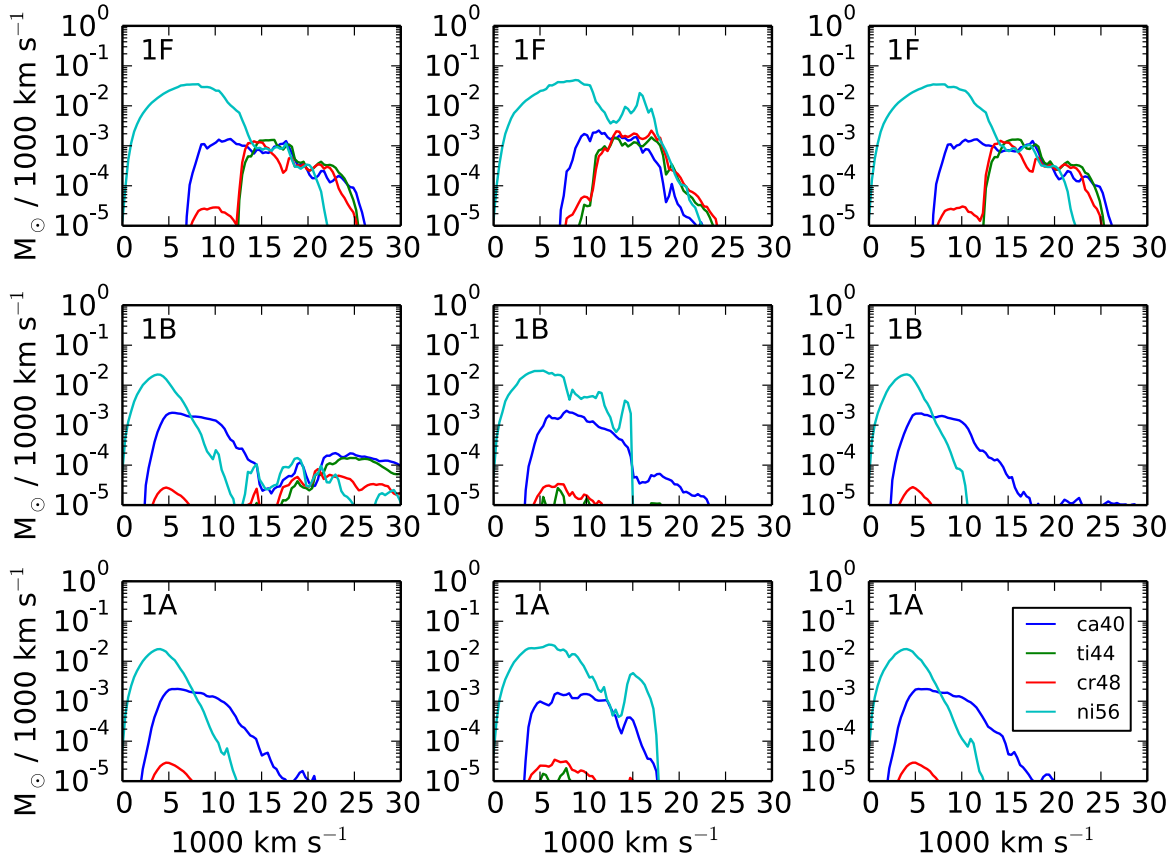


FIG. 6.— Velocity profiles of  $^{40}\text{Ca}$ ,  $^{44}\text{Ti}$ ,  $^{48}\text{Cr}$ ,  $^{56}\text{Ni}$  from three representing simulations. The simulations are for the cases: 1A - no helium, 1B - one WD with  $0.01M_{\odot}$  of helium, 1F - two WDs with  $0.1M_{\odot}$  of helium. Left: lower region with  $\cos \theta < -1/3$ . Middle: middle region with  $1/3 < \cos \theta < 1/3$ . Right: upper region with  $\cos \theta > 1/3$ . The angle  $\theta$  is the polar angle from the symmetry axis.

lowing  $^{44}\text{Ti}$  decay (see Perets 2014 for additional discussion of He-rich SNe contribution).

#### 4.3. The rate of WD-WD collisions

The rate of WD-WD collisions in dense stellar systems is low, and the overall rate was suggested to be dominated by possible WD-WD collisions in quasi-secular triples. Estimating the rate of WD-WD collisions is complicated and involves many uncertainties, both in the initial fractions and orbital parameters of triple systems as well as the effects of dynamical and stellar evolution. Such studies are beyond the scope of this paper which focuses on the properties of the explosions themselves. Nevertheless, one can constrain an upper limit on such rates through simple arguments (see also Soker et al. 2014).

Let us consider the most optimistic case. If we assume the binary components in wide binaries are formed independently (uncorrelated) then the mass-function of each stellar companion is independent. In such a case, the fraction of WD companions to WDs among WD-binaries is of the order of the overall WD fraction among single stars, namely  $\sim 10\%$ . If all of these were members of quasi-secular triple systems, with isotropic distribution of mutual inclinations between the inner and outer binaries of the triples, then  $\sim 5\%$  of these inner WD-WD binaries will collide due to quasi-secular evolution (Katz & Dong 2012), with about half of the collisions having impact parameter sufficiently small (smaller than half the WD radius), as to lead to a detonation and a full

thermonuclear explosion. In other words, 0.25% of WD systems will produce a thermonuclear explosion. Given that  $\sim 1\%$  of WD are required to explain the rates of type Ia SNe, then in the most optimistic and highly simplistic case WD collisions in triples can explain 25 % of type Ia SNe.

In practice, current available data suggest the rates are significantly smaller. Among  $0.9 - 1.5 M_{\odot}$  stars (constituting half of the potential WD progenitors in the mass range  $0.9 - 8 M_{\odot}$ ), the triple and higher multiplicity fraction is only 13% (Tokovinin 2014; Riddle et al. 2015). Moreover, among these, only a small fraction ( $< 10\%$ ) of the systems have period ratios residing in the quasi-secular regime ( $P_{\text{out}}/P_{\text{in}} < \sim 20$ ). Finally, there is reason to believe that the mutual inclinations of at least the shorter period triples ( $< 100$  yrs), are relatively small (Fekel 1981), rather than having an isotropic distribution. Such low inclination triples will not contribute at all to the quasi-secular regime. Taken together, one may conclude that WD progenitor systems in lower mass range may give rise to  $\sim 100$  times *smaller* rates than the most optimistic estimated rate considered above. Even allowing for a few times higher fractions due to some unaccounted-for incompleteness, these observational data already suggest very low rates. Moreover, some of the potential triple progenitors will induce a merger/collision of the inner binary before its evolution into a WD-WD binary. More massive stars are known to have higher multiplicity fractions (Duchêne & Kraus 2013; Sana et al. 2013), and the rates might therefore be

higher in the upper half of the mass range. However, such transition in the multiplicity and orbital properties with mass is likely to be continuous, and not produce orders of magnitude higher fractions of quasi-secular triples than those seen for the lower mass triples.

We conclude that the rate of WD-WD collisions is likely to give rise to only a small fraction of the type Ia SNe rate, of the order of at most a few percents of the total type Ia SN rate in the more optimistic case, and likely lower. Note, however, that the current data on triple and higher multiplicity systems are still very limited, and more data are needed in order provide better estimates, especially for collisions of more massive WDs.

## 5. SUMMARY

We investigated the result of head-on collisions of CO white dwarfs with a helium layers as a channel for type Ia supernovae. Pure CO WD-WD collisions were suggested in the past to be a channel for for type Ia in globular clusters (Benz et al. 1989; Rosswog et al. 2009) and more recently suggested as a channel for the production of type Ia SNe from triple systems (Thompson 2011; Katz & Dong 2012). Simulations of pure CO-WD collisions could have observational properties compatible with observed type Ia SNe in terms of the observed Iron elements abundances and energetics (Kushnir et al. 2013; García-Senz et al. 2013).

In this work we extend these studies to include WDs with a helium layer on at least one of the WDs. A low mass helium shell of mass up to  $M_{\text{He}} \leq 0.024M_{\odot}$  should exist in WDs according to current stellar evolution models. More massive helium shells can occur as a result of mass accretion from a companion. In these cases a quadruple system is probably needed to lead to a collision (as He-rich layer due to accretion requires a very close stellar companion).

We studied WD-WD collisions using the FLASH code, exploring a range of masses for both the WD CO bulk and for the outer Helium layers. We find that collisions involving low mass He-layers  $M_{\text{He}} = 0.01M_{\odot}$  give rise to He burning but no detonation occurs in the helium shell. The helium shell partially burns into intermediate elements resulting in a fast ejecta in the perpendicular plane to the collision. However, the He-burning does not affect the overall evolution of the collision and the CO-core detonation due to shock compression. In particular, the nickel yields are very similar to those obtained from pure CO-WD collisions. Nevertheless, high velocity ma-

terial rich with  $^{44}\text{Ti}$ , and  $^{48}\text{Cr}$  are produced at an order of magnitude higher levels than in pure CO-WD collision. We note that in general even pure CO WD-WD collisions produce more of such intermediate elements than single-degenerate models such as W7; the He-enriched collisions therefore produce up to two orders of magnitude higher levels of such intermediate elements compared with the single degenerate case.

Collisions with more massive He-layers ( $M_{\text{He}} = 0.024M_{\odot}$ ) due give rise to He-detonation, but the detonation front does not propagate much before the CO-core detonates due to shock compression, and the eventual outcomes of the collisions are still very similar to those obtained for of  $M_{\text{He}} = 0.01M_{\odot}$  cases.

When the more He-rich collisions are considered ( $M_{\text{He}} = 0.1M_{\odot}$ ; models 1F,2E) the helium layer is sufficiently thick as to enable the helium detonation wave to propagate along the WD helium-shell. The helium shell is burned mostly to intermediate elements and ejected with lower velocities before a detonation is triggered in the CO core. The CO detonation itself is still triggered by the shock compression and behaves similarly to the case of pure CO-WD collisions, with almost no effect of the helium burning itself on the CO detonation. The nickel yields in this case are also similar to that of pure CO-WDs collisions. The CO explosion ejects material with velocities higher than that in ejected burned helium shell. This results with a second shock wave accelerating the burned helium material to higher velocities. Finally, in the most He-rich cases ( $M_{\text{He}} = 0.2M_{\odot}$ ; model 1G), a converging shock from the helium detonation is able to detonate the CO-core earlier, before the shock compression due to the collision, resulting in a lower production of Iron elements.

We conclude that WD-WD collisions with He-layers may affect the outcome of WD-WD collisions and give rise to significant composition changes, as well as possible kinematic and morphological changes, which can become significant for the most He-rich WD-WD collisions. We note that after the submission of the current paper Holcomb & Kushnir (2015) studied these issues, finding similar outcomes and further confirming our results.

HBP acknowledges support by the ISF I-CORE grant 1829/12 and the Technion Deloro fellowship. The software used in this work was in part developed by the DOE NNSA-ASC OASCR Flash Center at the University of Chicago.

## REFERENCES

- Antonini, F. & Perets, H. B. 2012, *ApJ*, 757, 27  
Benz, W., Thielemann, F.-K., & Hills, J. G. 1989, *ApJ*, 342, 986  
Bildsten, L., Shen, K. J., Weinberg, N. N., & Nelemans, G. 2007, *ApJ*, 662, L95  
Cyburt, R. H., Amthor, A. M., Ferguson, R., Meisel, Z., Smith, K., Warren, S., Heger, A., Hoffman, R. D., Rauscher, T., Sakharuk, A., Schatz, H., Thielemann, F. K., & Wiescher, M. 2010, *ApJS*, 189, 240  
Duchêne, G. & Kraus, A. 2013, *ARA&A*, 51, 269  
Fekel, Jr., F. C. 1981, *ApJ*, 246, 879  
Fryxell, B., Olson, K., Ricker, P., Timmes, F. X., Zingale, M., Lamb, D. Q., MacNeice, P., Rosner, R., Truran, J. W., & Tufo, H. 2000, *ApJS*, 131, 273  
García-Senz, D., Cabezón, R. M., Arcones, A., Relaño, A., & Thielemann, F. K. 2013, *MNRAS*, 436, 3413  
Hamers, A. S., Pols, O. R., Claeys, J. S. W., & Nelemans, G. 2013, *MNRAS*, 430, 2262  
Hawley, W. P., Athanassiadou, T., & Timmes, F. X. 2012, *ApJ*, 759, 39  
Holcomb, C. & Kushnir, D. 2015, *ArXiv e-prints*  
Jordan, IV, G. C., Perets, H. B., Fisher, R. T., & van Rossum, D. R. 2012, *ApJ*, 761, L23  
Kashi, A. & Soker, N. 2011, *MNRAS*, 417, 1466  
Katz, B. & Dong, S. 2012, *ArXiv e-prints*  
Kozai, Y. 1962, *AJ*, 67, 591  
Kromer, M., Fink, M., Stanishev, V., Taubenberger, S., Ciaraldi-Schoolman, F., Pakmor, R., Röpke, F. K., Ruiter, A. J., Seitenzahl, I. R., Sim, S. A., Blanc, G., Elias-Rosa, N., & Hillebrandt, W. 2013, *MNRAS*, 429, 2287  
Krzemiński, W. 1972, *Acta Astron*, 22, 387

- Kushnir, D. & Katz, B. 2014, *ApJ*, 785, 124
- Kushnir, D., Katz, B., Dong, S., Livne, E., & Fernández, R. 2013, *ApJ*, 778, L37
- Lawlor, T. M. & MacDonald, J. 2006, *MNRAS*, 371, 263
- Lidov, M. L. 1962, *Planet. Space Sci.*, 9, 719
- Livio, M. & Riess, A. G. 2003, *ApJ*, 594, L93
- Livne, E. & Glasner, A. S. 1991, *ApJ*, 370, 272
- Lopez, L. A., Grefenstette, B. W., Reynolds, S. P., An, H., Boggs, S. E., Christensen, F. E., Craig, W. W., Eriksen, K. A., Fryer, C. L., Hailey, C. J., Harrison, F. A., Madsen, K. K., Stern, D. K., Zhang, W. W., & Zoglauer, A. 2015, *ApJ*, 814, 132
- Lorén-Aguilar, P., Isern, J., & García-Berro, E. 2010, *MNRAS*, 406, 2749
- Maoz, D., Mannucci, F., & Nelemans, G. 2014, *ARA&A*, 52, 107
- Michael, E. & Perets, H. B. 2015, *ArXiv e-prints*
- Nomoto, K., Thielemann, F.-K., & Yokoi, K. 1984, *ApJ*, 286, 644
- Pakmor, R., Kromer, M., Taubenberger, S., & Springel, V. 2013, *ApJ*, 770, L8
- Paxton, B., Bildsten, L., Dotter, A., Herwig, F., Lesaffre, P., & Timmes, F. 2011, *ApJS*, 192, 3
- Paxton, B., Marchant, P., Schwab, J., Bauer, E. B., Bildsten, L., Cantiello, M., Dessart, L., Farmer, R., Hu, H., Langer, N., Townsend, R. H. D., Townsley, D. M., & Timmes, F. X. 2015, *ApJS*, 220, 15
- Perets, H. B. 2014, *ArXiv e-prints*
- Perets, H. B., Gal-Yam, A., Mazzali, P. A., Arnett, D., Kagan, D., Filippenko, A. V., Li, W., Arcavi, I., Cenko, S. B., Fox, D. B., Leonard, D. C., Moon, D.-S., Sand, D. J., Soderberg, A. M., Anderson, J. P., James, P. A., Foley, R. J., Ganeshalingam, M., Ofek, E. O., Bildsten, L., Nelemans, G., Shen, K. J., Weinberg, N. N., Metzger, B. D., Piro, A. L., Quataert, E., Kiewe, M., & Poznanski, D. 2010, *Nature*, 465, 322
- Raskin, C., Scannapieco, E., Fryer, C., Rockefeller, G., & Timmes, F. X. 2012, *ApJ*, 746, 62
- Raskin, C., Scannapieco, E., Rockefeller, G., Fryer, C., Diehl, S., & Timmes, F. X. 2010, *ApJ*, 724, 111
- Raskin, C., Timmes, F. X., Scannapieco, E., Diehl, S., & Fryer, C. 2009, *MNRAS*, 399, L156
- Riddle, R. L., Tokovinin, A., Mason, B. D., Hartkopf, W. I., Roberts, Jr., L. C., Baranec, C., Law, N. M., Bui, K., Burse, M. P., Das, H. K., Dekany, R. G., Kulkarni, S., Punnadi, S., Ramaprakash, A. N., & Tendulkar, S. P. 2015, *ApJ*, 799, 4
- Rosswog, S., Kasen, D., Guillochon, J., & Ramirez-Ruiz, E. 2009, *ApJ*, 705, L128
- Sana, H., de Koter, A., de Mink, S. E., Dunstall, P. R., Evans, C. J., Hénault-Brunet, V., Maíz Apellániz, J., Ramírez-Agudelo, O. H., Taylor, W. D., Walborn, N. R., Clark, J. S., Crowther, P. A., Herrero, A., Gieles, M., Langer, N., Lennon, D. J., & Vink, J. S. 2013, *A&A*, 550, A107
- Shen, K. J. & Bildsten, L. 2009, *ApJ*, 699, 1365
- . 2014, *ApJ*, 785, 61
- Soker, N., García-Berro, E., & Althaus, L. G. 2014, *MNRAS*, 437, L66
- Thompson, T. A. 2011, *ApJ*, 741, 82
- Timmes, F. X., Hoffman, R. D., & Woosley, S. E. 2000, *ApJS*, 129, 377
- Timmes, F. X. & Swesty, F. D. 2000, *ApJS*, 126, 501
- Tokovinin, A. 2014, *AJ*, 147, 87
- Troja, E., Segreto, A., La Parola, V., Hartmann, D., Baumgartner, W., Markwardt, C., Barthelmy, S., Cusumano, G., & Gehrels, N. 2014, *ApJ*, 797, L6
- Waldman, R., Sauer, D., Livne, E., Perets, H., Glasner, A., Mazzali, P., Truran, J. W., & Gal-Yam, A. 2011, *ApJ*, 738, 21
- Wolf, W. M., Bildsten, L., Brooks, J., & Paxton, B. 2013, *ApJ*, 777, 136
- Woosley, S. E., Taam, R. E., & Weaver, T. A. 1986, *ApJ*, 301, 601



Isotope	1A	1C	Isotope	1A	1C
<sup>1</sup> H	2.23e-04	2.25e-04	<sup>237</sup> Pu	4.63e-08	3.37e-08
<sup>2</sup> H	2.95e-16	2.30e-35	<sup>238</sup> Pu	4.19e-10	2.18e-07
<sup>3</sup> He	3.55e-16	6.29e-17	<sup>239</sup> Pu	3.59e-09	5.68e-04
<sup>4</sup> He	1.71e-13	1.89e-13	<sup>240</sup> Pu	2.15e-13	1.27e-05
<sup>6</sup> Li	5.47e-03	5.55e-03	<sup>241</sup> Pu	6.15e-18	1.03e-17
<sup>7</sup> Li	1.72e-15	5.93e-16	<sup>242</sup> Pu	3.03e-24	1.29e-33
<sup>9</sup> Be	2.01e-10	2.01e-10	<sup>243</sup> Pu	3.69e-27	1.95e-34
<sup>10</sup> Be	4.35e-15	2.28e-15	<sup>244</sup> Pu	6.37e-29	6.39e-35
<sup>11</sup> B	9.10e-22	1.55e-23	<sup>245</sup> Pu	6.49e-29	2.99e-36
<sup>12</sup> B	3.15e-13	4.12e-19	<sup>246</sup> Pu	2.14e-07	6.59e-33
<sup>13</sup> C	5.04e-02	9.25e-02	<sup>247</sup> Pu	7.97e-09	3.02e-28
<sup>14</sup> C	3.54e-10	3.89e-08	<sup>248</sup> Pu	2.30e-08	2.30e-20
<sup>15</sup> N	4.57e-08	2.84e-34	<sup>249</sup> Pu	2.29e-14	1.73e-14
<sup>16</sup> N	1.12e-07	1.49e-06	<sup>250</sup> Pu	9.53e-14	7.69e-08
<sup>17</sup> N	4.58e-09	1.03e-07	<sup>251</sup> Pu	3.11e-19	8.59e-34
<sup>18</sup> O	1.67e-06	3.64e-35	<sup>252</sup> Pu	7.24e-24	3.61e-34
<sup>19</sup> O	1.33e-07	6.74e-35	<sup>253</sup> Pu	2.99e-28	1.98e-34
<sup>20</sup> O	1.01e-01	1.26e-01	<sup>254</sup> Pu	4.44e-26	1.33e-35
<sup>21</sup> O	4.66e-09	1.18e-07	<sup>255</sup> Pu	6.73e-29	4.46e-37
<sup>22</sup> O	1.69e-12	8.95e-10	<sup>256</sup> Pu	7.07e-11	8.67e-37
<sup>23</sup> F	1.20e-07	4.04e-35	<sup>257</sup> Pu	5.91e-04	1.05e-31
<sup>24</sup> F	5.41e-09	8.97e-33	<sup>258</sup> Pu	1.36e-05	4.42e-33
<sup>25</sup> F	2.63e-10	1.95e-09	<sup>259</sup> Pu	4.37e-07	3.01e-07
<sup>26</sup> Ne	2.79e-09	1.11e-36	<sup>260</sup> Pu	5.00e-10	1.04e-29
<sup>27</sup> Ne	1.80e-09	1.21e-35	<sup>261</sup> Pu	7.46e-09	9.35e-03
<sup>28</sup> Ne	1.04e-03	9.04e-04	<sup>262</sup> Pu	2.31e-12	3.17e-04
<sup>29</sup> Ne	3.32e-09	3.03e-09	<sup>263</sup> Pu	2.84e-17	2.12e-13
<sup>30</sup> Ne	3.35e-13	3.10e-13	<sup>264</sup> Pu	7.83e-24	8.49e-34
<sup>31</sup> Na	1.25e-06	2.74e-06	<sup>265</sup> Pu	1.33e-26	1.46e-33
<sup>32</sup> Na	1.01e-13	3.75e-32	<sup>266</sup> Pu	7.37e-26	8.05e-26
<sup>33</sup> Mg	1.94e-06	9.59e-36	<sup>267</sup> Pu	6.96e-29	2.52e-26
<sup>34</sup> Mg	2.87e-03	2.15e-03	<sup>268</sup> Pu	9.00e-08	1.00e-32
<sup>35</sup> Mg	1.10e-06	9.41e-07	<sup>269</sup> Pu	9.26e-07	1.31e-30
<sup>36</sup> Al	4.59e-06	4.04e-06	<sup>270</sup> Pu	2.87e-06	6.65e-16
<sup>37</sup> Al	4.77e-07	4.13e-36	<sup>271</sup> Pu	2.91e-13	7.41e-23
<sup>38</sup> Si	3.10e-01	2.79e-01	<sup>272</sup> Pu	2.17e-13	1.87e-06
<sup>39</sup> Si	6.86e-05	4.31e-05	<sup>273</sup> Pu	5.27e-19	5.29e-32
<sup>40</sup> P	2.35e-05	2.23e-05	<sup>274</sup> Pu	2.98e-15	5.74e-37
<sup>41</sup> P	4.76e-06	2.94e-36	<sup>275</sup> Pu	9.79e-03	4.68e-32
<sup>42</sup> S	1.94e-01	1.78e-01	<sup>276</sup> Pu	3.30e-04	9.91e-34
<sup>43</sup> Cl	2.69e-06	2.53e-06	<sup>277</sup> Pu	7.49e-06	6.12e-06
<sup>44</sup> Cl	9.00e-10	3.08e-23	<sup>278</sup> Pu	7.98e-09	4.12e-28
<sup>45</sup> Cl	1.27e-09	2.96e-06	<sup>279</sup> Pu	3.62e-05	4.21e-01
<sup>46</sup> Cl	6.05e-17	3.02e-33	<sup>280</sup> Pu	9.12e-07	4.55e-03
<sup>47</sup> Ar	2.23e-07	2.30e-36	<sup>281</sup> Pu	1.47e-15	1.81e-13
<sup>48</sup> Ar	4.14e-02	3.82e-02	<sup>282</sup> Pu	2.73e-21	4.88e-30
<sup>49</sup> Ar	4.47e-06	2.99e-27	<sup>283</sup> Pu	1.40e-18	1.04e-28
<sup>50</sup> Ar	5.26e-07	3.55e-07	<sup>284</sup> Pu	6.42e-21	8.03e-34
<sup>51</sup> Ar	7.42e-13	3.29e-26	<sup>285</sup> Pu	3.02e-16	1.55e-34
<sup>52</sup> Ar	6.97e-15	1.70e-12	<sup>286</sup> Pu	1.87e-21	1.42e-35
<sup>53</sup> Ar	2.72e-21	9.15e-33	<sup>287</sup> Pu	4.14e-17	4.72e-36
<sup>54</sup> K	1.79e-06	1.33e-06	<sup>288</sup> Pu	1.56e-23	1.94e-36
<sup>55</sup> K	3.02e-11	3.25e-12	<sup>289</sup> Pu	7.95e-29	1.07e-36
<sup>56</sup> K	3.01e-12	5.61e-07	<sup>290</sup> Pu	1.53e-06	2.15e-31
<sup>57</sup> K	4.00e-17	5.48e-32	<sup>291</sup> Pu	9.30e-07	1.58e-29
<sup>58</sup> K	5.11e-21	9.72e-32	<sup>292</sup> Pu	7.98e-08	4.85e-20
<sup>59</sup> K	3.79e-26	2.11e-33	<sup>293</sup> Pu	2.93e-13	2.34e-23
<sup>60</sup> Ca	3.16e-09	1.24e-36	<sup>294</sup> Pu	8.84e-11	2.46e-07
<sup>61</sup> Ca	4.04e-02	3.75e-02	<sup>295</sup> Pu	1.09e-17	7.92e-29
<sup>62</sup> Ca	7.73e-07	3.36e-20	<sup>296</sup> Pu	1.63e-17	2.47e-32
<sup>63</sup> Ca	1.41e-08	9.59e-09	<sup>297</sup> Pu	2.89e-17	4.11e-34
<sup>64</sup> Ca	1.23e-10	2.57e-07	<sup>298</sup> Pu	2.15e-16	1.27e-34
<sup>65</sup> Ca	2.44e-09	4.92e-05	<sup>299</sup> Pu	9.01e-18	1.42e-36
<sup>66</sup> Ca	3.37e-17	1.55e-28	<sup>300</sup> Pu	2.34e-21	5.56e-36
<sup>67</sup> Ca	5.38e-20	2.85e-16	<sup>301</sup> Pu	7.94e-29	9.74e-37
<sup>68</sup> Ca	3.35e-25	4.64e-31	<sup>302</sup> Pu	8.06e-29	1.05e-36
<sup>69</sup> Ca	3.96e-27	1.73e-26	<sup>303</sup> Pu	9.23e-19	4.16e-37
<sup>70</sup> Ca	5.94e-29	9.37e-34	<sup>304</sup> Pu	4.33e-01	7.27e-31
<sup>71</sup> Sc	2.53e-07	3.92e-32	<sup>305</sup> Pu	4.55e-03	1.99e-31
<sup>72</sup> Sc	1.17e-11	2.06e-32	<sup>306</sup> Pu	4.58e-03	4.62e-03
<sup>73</sup> Sc	3.95e-11	5.63e-08	<sup>307</sup> Pu	2.43e-07	1.62e-18
<sup>74</sup> Sc	8.90e-16	3.66e-30	<sup>308</sup> Pu	3.41e-09	3.31e-09
<sup>75</sup> Sc	8.91e-18	6.71e-31	<sup>309</sup> Pu	9.04e-14	5.07e-14
<sup>76</sup> Sc	4.12e-22	2.02e-31	<sup>310</sup> Pu	3.18e-14	2.17e-14
<sup>77</sup> Sc	4.04e-24	1.18e-32	<sup>311</sup> Pu	5.75e-17	2.72e-16
<sup>78</sup> Sc	6.01e-29	1.88e-34	<sup>312</sup> Pu	1.09e-15	1.15e-15
<sup>79</sup> Sc	6.12e-29	2.33e-35	<sup>313</sup> Pu	1.17e-19	1.11e-19
<sup>80</sup> Ti	3.72e-11	8.07e-37	<sup>314</sup> Pu	4.87e-21	3.53e-20
<sup>81</sup> Ti	5.10e-05	5.32e-29	<sup>315</sup> Pu	1.26e-24	3.00e-24
<sup>82</sup> Ti	6.82e-08	1.63e-32	<sup>316</sup> Pu	2.12e-27	2.12e-27
<sup>83</sup> Ti			<sup>317</sup> Pu		
<sup>84</sup> Ti			<sup>318</sup> Pu		
<sup>85</sup> Ti			<sup>319</sup> Pu		
<sup>86</sup> Ti			<sup>320</sup> Pu		
<sup>87</sup> Ti			<sup>321</sup> Pu		
<sup>88</sup> Ti			<sup>322</sup> Pu		
<sup>89</sup> Ti			<sup>323</sup> Pu		
<sup>90</sup> Ti			<sup>324</sup> Pu		
<sup>91</sup> Ti			<sup>325</sup> Pu		
<sup>92</sup> Ti			<sup>326</sup> Pu		
<sup>93</sup> Ti			<sup>327</sup> Pu		
<sup>94</sup> Ti			<sup>328</sup> Pu		
<sup>95</sup> Ti			<sup>329</sup> Pu		
<sup>96</sup> Ti			<sup>330</sup> Pu		
<sup>97</sup> Ti			<sup>331</sup> Pu		
<sup>98</sup> Ti			<sup>332</sup> Pu		
<sup>99</sup> Ti			<sup>333</sup> Pu		
<sup>100</sup> Ti			<sup>334</sup> Pu		
<sup>101</sup> Ti			<sup>335</sup> Pu		
<sup>102</sup> Ti			<sup>336</sup> Pu		
<sup>103</sup> Ti			<sup>337</sup> Pu		
<sup>104</sup> Ti			<sup>338</sup> Pu		
<sup>105</sup> Ti			<sup>339</sup> Pu		
<sup>106</sup> Ti			<sup>340</sup> Pu		
<sup>107</sup> Ti			<sup>341</sup> Pu		
<sup>108</sup> Ti			<sup>342</sup> Pu		
<sup>109</sup> Ti			<sup>343</sup> Pu		
<sup>110</sup> Ti			<sup>344</sup> Pu		
<sup>111</sup> Ti			<sup>345</sup> Pu		
<sup>112</sup> Ti			<sup>346</sup> Pu		
<sup>113</sup> Ti			<sup>347</sup> Pu		
<sup>114</sup> Ti			<sup>348</sup> Pu		
<sup>115</sup> Ti			<sup>349</sup> Pu		
<sup>116</sup> Ti			<sup>350</sup> Pu		
<sup>117</sup> Ti			<sup>351</sup> Pu		
<sup>118</sup> Ti			<sup>352</sup> Pu		
<sup>119</sup> Ti			<sup>353</sup> Pu		
<sup>120</sup> Ti			<sup>354</sup> Pu		
<sup>121</sup> Ti			<sup>355</sup> Pu		
<sup>122</sup> Ti			<sup>356</sup> Pu		
<sup>123</sup> Ti			<sup>357</sup> Pu		
<sup>124</sup> Ti			<sup>358</sup> Pu		
<sup>125</sup> Ti			<sup>359</sup> Pu		
<sup>126</sup> Ti			<sup>360</sup> Pu		
<sup>127</sup> Ti			<sup>361</sup> Pu		
<sup>128</sup> Ti			<sup>362</sup> Pu		
<sup>129</sup> Ti			<sup>363</sup> Pu		
<sup>130</sup> Ti			<sup>364</sup> Pu		
<sup>131</sup> Ti			<sup>365</sup> Pu		
<sup>132</sup> Ti			<sup>366</sup> Pu		
<sup>133</sup> Ti			<sup>367</sup> Pu		
<sup>134</sup> Ti			<sup>368</sup> Pu		
<sup>135</sup> Ti			<sup>369</sup> Pu		
<sup>136</sup> Ti			<sup>370</sup> Pu		
<sup>137</sup> Ti			<sup>371</sup> Pu		
<sup>138</sup> Ti			<sup>372</sup> Pu		
<sup>139</sup> Ti			<sup>373</sup> Pu		
<sup>140</sup> Ti			<sup>374</sup> Pu		
<sup>141</sup> Ti			<sup>375</sup> Pu		
<sup>142</sup> Ti			<sup>376</sup> Pu		
<sup>143</sup> Ti			<sup>377</sup> Pu		
<sup>144</sup> Ti			<sup>378</sup> Pu		
<sup>145</sup> Ti			<sup>379</sup> Pu		
<sup>146</sup> Ti			<sup>380</sup> Pu		
<sup>147</sup> Ti			<sup>381</sup> Pu		
<sup>148</sup> Ti			<sup>382</sup> Pu		
<sup>149</sup> Ti			<sup>383</sup> Pu		
<sup>150</sup> Ti			<sup>384</sup> Pu		
<sup>151</sup> Ti			<sup>385</sup> Pu		
<sup>152</sup> Ti			<sup>386</sup> Pu		
<sup>153</sup> Ti			<sup>387</sup> Pu		
<sup>154</sup> Ti			<sup>388</sup> Pu		
<sup>155</sup> Ti			<sup>389</sup> Pu		
<sup>156</sup> Ti			<sup>390</sup> Pu		
<sup>157</sup> Ti			<sup>391</sup> Pu		
<sup>158</sup> Ti			<sup>392</sup> Pu		
<sup>159</sup> Ti			<sup>393</sup> Pu		
<sup>160</sup> Ti			<sup>394</sup> Pu		
<sup>161</sup> Ti			<sup>395</sup> Pu		
<sup>162</sup> Ti			<sup>396</sup> Pu		
<sup>163</sup> Ti			<sup>397</sup> Pu		
<sup>164</sup> Ti			<sup>398</sup> Pu		
<sup>165</sup> Ti			<sup>399</sup> Pu		
<sup>166</sup> Ti			<sup>400</sup> Pu		
<sup>167</sup> Ti			<sup>401</sup> Pu		
<sup>168</sup> Ti			<sup>402</sup> Pu		
<sup>169</sup> Ti			<sup>403</sup> Pu		
<sup>170</sup> Ti			<sup>404</sup> Pu		
<sup>171</sup> Ti			<sup>405</sup> Pu		
<sup>172</sup> Ti			<sup>406</sup> Pu		
<sup>173</sup> Ti			<sup>407</sup> Pu		
<sup>174</sup> Ti			<sup>408</sup> Pu		
<sup>175</sup> Ti			<sup>409</sup> Pu		
<sup>176</sup> Ti			<sup>410</sup> Pu		
<sup>177</sup> Ti			<sup>411</sup> Pu		
<sup>178</sup> Ti			<sup>412</sup> Pu		
<sup>179</sup> Ti			<sup>413</sup> Pu		
<sup>180</sup> Ti			<sup>414</sup> Pu		
<sup>181</sup> Ti			<sup>415</sup> Pu		
<sup>182</sup> Ti			<sup>416</sup> Pu		
<sup>183</sup> Ti			<sup>417</sup> Pu		
<sup>184</sup> Ti			<sup>418</sup> Pu		
<sup>185</sup> Ti			<sup>419</sup> Pu		
<sup>186</sup> Ti			<sup>420</sup> Pu		
<sup>187</sup> Ti			<sup>421</sup> Pu		
<sup>188</sup> Ti			<sup>422</sup> Pu		
<sup>189</sup> Ti			<sup>423</sup> Pu		
<sup>190</sup> Ti			<sup>424</sup> Pu		
<sup>191</sup> Ti			<sup>425</sup> Pu		
<sup>192</sup> Ti			<sup>426</sup> Pu		
<sup>193</sup> Ti			<sup>427</sup> Pu		
<sup>194</sup> Ti			<sup>428</sup> Pu		
<sup>195</sup> Ti			<sup>429</sup> Pu		
<sup>196</sup> Ti			<sup>430</sup> Pu		
<sup>197</sup> Ti					